TOXICOLOGICAL SCIENCES, 166(2), 2018, 306–317

doi: 10.1093/toxsci/kfy214
Advance Access Publication Date: August 27, 2018
Research Article

Niclosamide Induces Epiboly Delay During Early Zebrafish Embryogenesis

Sara M. Vliet,* Subham Dasgupta,* and David C. Volz*,[1]

*Department of Environmental Sciences, University of California, Riverside, California 92521

[1]To whom correspondence should be addressed. Fax: (951) 827-3993. E-mail: david.volz@ucr.edu.

ABSTRACT

Niclosamide is an antihelminthic drug used worldwide for the treatment of tapeworm infections. Recent drug repurposing screens have revealed that niclosamide exhibits diverse mechanisms of action and, as a result, demonstrates promise for a number of applications, including the treatment of cancer, bacterial infections, and Zika virus. As new applications of niclosamide will require non-oral delivery routes that may lead to exposure *in utero*, the objective of this study was to investigate the mechanism of niclosamide toxicity during early stages of embryonic development. Using zebrafish as a model, we found that niclosamide induced a concentration-dependent delay in epiboly progression during late-blastula and early-gastrula, an effect that was dependent on exposure during the maternal-to-zygotic transition—a period characterized by degradation of maternally derived transcripts, zygotic genome activation, and initiation of cell motility. Moreover, we found that niclosamide did not affect embryonic oxygen consumption, suggesting that oxidative phosphorylation—a well-established target for niclosamide within intestinal parasites—may not play a role in niclosamide-induced epiboly delay. However, mRNA-sequencing revealed that niclosamide exposure during blastula and early-gastrula significantly impacted the timing of zygotic genome activation as well as the abundance of cytoskeleton- and cell cycle regulation-specific transcripts. In addition, we found that niclosamide inhibited tubulin polymerization *in vitro*, suggesting that niclosamide-induced delays in epiboly progression may, in part, be driven by disruption of microtubule formation and cell motility within the developing embryo.

Key words: niclosamide; zebrafish; epiboly; development; cytoskeleton.

Niclosamide (2′,5-dichloro-4-nitro salicylanilide) is an oral antihelminthic drug that is approved by the U.S. Food and Drug Administration and has been used since the 1960s for treatment of tapeworm infections in humans and animals (Andrews *et al.*, 1982). Oral doses of niclosamide are well-tolerated and result in minimal side effects, an outcome that is due to low niclosamide absorption from the gastrointestinal tract to systemic circulation as well as rapid elimination and minimal bioaccumulation of any absorbed niclosamide (Andrews *et al.*, 1982; Duhm *et al.*, 1961). Based on studies conducted to date, niclosamide is not suspected to result in birth defects or cause developmental toxicity, teratogenicity, mutagenicity, or carcinogenicity, although the majority of animal studies supporting these conclusions relied on the use of oral doses of a niclosamide formulation that limits absorption within the gastrointestinal tract. Nevertheless, niclosamide should only be used by pregnant women when justified, and use in the first trimester of pregnancy should only occur when absolutely necessary (Andrews *et al.*, 1982).

The antiparasitic activity of niclosamide was first reported to be mediated through inhibition of mitochondrial oxidative phosphorylation (OXPHOS) and ATP production (Andrews *et al.*, 1982; Weinbach and Garbus, 1969). This hypothesis was based on studies demonstrating that niclosamide exhibited uncoupling activity in isolated mitochondria (Tao *et al.*, 2014; Yorke and Turton, 1974) as well as *in vivo* uncoupling measured by increased oxygen consumption in mice and invertebrates (Raheem *et al.*, 1980; Tao *et al.*, 2014). Niclosamide has also been reported to inhibit the conversion of NADH to NAD+ within tapeworms (Park and Fioravanti, 2006) and increase intracellular reactive oxygen species and apoptosis in cell-based assays (Jin *et al.*, 2010; Lee *et al.*, 2014).

Recent drug repurposing screens have shown that niclosamide may be effective for treating a broad range of illnesses such as cancer (Chen *et al.*, 2018; Li *et al.*, 2014; Pan *et al.*, 2012), bacterial infections (Gwisai *et al.*, 2017; Imperi *et al.*, 2013; Rajamuthiah *et al.*, 2015; Tharmalingam *et al.*, 2018), and Zika virus (Cairns *et al.*, 2018; Li *et al.*, 2017; Xu *et al.*, 2016). Although the mechanisms underlying these potential off-label uses remain largely unknown, these studies have reported that niclosamide has the potential to disrupt multiple signaling pathways including NF-κB, Wnt/β-catenin, STAT3, mTORC1, and Notch (Balgi *et al.*, 2009; Chen *et al.*, 2009; Jin *et al.*, 2010; Ren *et al.*, 2010; Suliman *et al.*, 2016). Overall, the diversity of literature and observed effects of niclosamide exposure suggest that the mechanisms responsible for many therapeutic (as well as toxic) effects are likely complex and may not be directly related to the activity of niclosamide as an inhibitor of mitochondrial function.

The low systemic bioavailability of niclosamide though oral administration—although key to its success as an antihelminthic—may prove to be a challenge for many of the proposed off-label uses. Therefore, new routes of exposure with increased absorption will be essential for the future success of niclosamide in treating various conditions within humans (Li *et al.*, 2014; Lu *et al.*, 2016). In addition, the broad range of uses for niclosamide currently being discussed introduces the possibility for *in utero* exposure within human populations. Therefore, there is a need to reevaluate the toxicity of niclosamide within a developmental context. In 2017, we carried out a high-content screen of the LOPAC^{1280} (Library of Pharmacologically Active Compounds) library—a commercially available library of 1280 marketed drugs, failed development candidates, and well-characterized small molecules widely used for validation of high-throughput screening assays. Based on this screen, niclosamide was one of the most potent developmental toxicants within zebrafish embryos during the first 25 h of development (Vliet *et al.*, 2017), with exposure to 10 μM niclosamide from 5 to 25 h post-fertilization (hpf) resulting in 100% embryo mortality (Vliet *et al.*, 2017). Therefore, the overall objective of this study was to investigate the mechanism of toxicity of niclosamide at lower, non-lethal concentrations during early stages of embryonic development.

MATERIALS AND METHODS

Animals

Adult *fli1:egfp* zebrafish were maintained and bred on a recirculating system using previously described procedures (Vliet *et al.*, 2017). We relied on *fli1:egfp* zebrafish for this study, as we originally identified niclosamide as a potential developmental toxicant using this strain (Vliet *et al.*, 2017). For all experiments, newly fertilized eggs were collected within 30 min of spawning, rinsed, and reared in a temperature-controlled incubator at 28°C under a 14:10-h light-dark cycle. All embryos were sorted and staged according to previously described methods (Kimmel *et al.*, 1995). All adult breeders were handled and treated in accordance with an Institutional Animal Care and Use Committee (IACUC)-approved animal use protocol (20150035) at the University of California, Riverside.

Chemicals

Niclosamide (≥98%) was purchased from Sigma-Aldrich. Stock solutions were prepared in high performance liquid chromatography (HPLC)-grade dimethyl sulfoxide (DMSO), and stored within 2-ml amber glass vials with polytetrafluoroethylene-lined caps. Working solutions were prepared in embryo media (5 mM NaCl, 0.17 mM KCl, 0.33 mM $CaCl_2$, 0.33 mM $MgSO_4$, pH 7) immediately prior to each experiment.

Phenotypic assessments

The magnitude of niclosamide-induced epiboly delay within zebrafish embryos was assessed by exposing embryos (10 embryos per petri dish; three replicate petri dishes per treatment) from 2 to 6 hpf under static conditions at 28°C to 3 ml of vehicle (0.1% DMSO) or niclosamide concentrations (0.078–0.625 μM) that resulted in epiboly delay in the absence of mortality. At 6 hpf, embryos were removed from treatment solution, arranged laterally in an agarose mold, and imaged using a Leica MZ10 F stereomicroscope equipped with a DMC2900 camera. The height of the cell mass and percent epiboly—calculated as (cell mass progression over yolk sac)/yolk sac height*100—were measured for each embryo using ImageJ (v1.51m9).

To assess embryo recovery and identify potential sensitive windows of exposure, embryos (10 embryos per petri dish; three replicate petri dishes per treatment) were exposed under static conditions at 28°C to 3 ml of vehicle (0.1% DMSO) or niclosamide (0.156, 0.313, and 0.625 μM) beginning at 2 hpf. Every hour until 6 hpf, embryos were removed from the exposure dish by aspirating treatment solution and transferring to clean embryo media. At 6 hpf, all embryos were imaged using procedures described above. To identify possible sensitive windows of exposure, exposures were carried out under similar conditions as the recovery assay, with exposures beginning every hour until 5 hpf.

To investigate the effect of early developmental niclosamide exposure on later stages of development, the effect of niclosamide-induced epiboly delay on 24-hpf embryos was assessed by exposing embryos (10 embryos per petri dish; three replicate petri dishes per treatment) under static conditions at 28°C to 3 ml of vehicle (0.1% DMSO) or niclosamide (0.313 μM) at time points equivalent to recovery and sensitive window assays. At 6 hpf, embryos were transferred to replicate petri dishes containing clean embryo media and incubated at 28°C until 24 hpf. At 24 hpf, viable embryos were arrayed into a 384-well plate, resulting in one embryo per well and 16 embryos per treatment; the plate was then centrifuged for 2 min at 200 rpm to ensure all embryos were positioned at the well bottom. Using previously described procedures (Vliet *et al.*, 2017), embryos were imaged on our ImageXpress Micro XLS Widefield High-Content Screening System and total body area was analyzed within MetaXpress 6.0.3.1658 (Molecular Devices, Sunnyvale, California) as a readout for embryonic growth. Briefly, a 4× objective and FITC filter cube was used to acquire one frame per entire well because eGFP is expressed along the anteroposterior axis of 24-hpf *fli1:egfp* embryos. Total body area was then quantified within MetaXpress using automated custom journal scripts that (1) creates a threshold for each FITC-specific embryo image; (2) measures total area of the threshold for each embryo; and (3) exports total area data for each embryo to an Excel spreadsheet.

Oxygen consumption assay

We used 2-ml glass vials containing oxygen-sensitive sensors to monitor oxygen concentrations within the surrounding embryo media using a SDR SensorDish Reader (PreSens Precision Sensing GmbH, Regensburg, Germany). Embryos were exposed to vehicle (0.1% DMSO) or niclosamide (0.156–0.625 μM) in

groups of 10 embryos per petri dish from 2 to 6 hpf under static conditions at 28°C. At 6 hpf, embryos were rinsed three times with clean embryo media and placed into equilibrated sensor vials containing clean embryo media at a density of 20 embryos per vial, with four-independent replicate vials per treatment. Oxygen concentrations were then measured at 28°C in a dark incubator over the course of 400 min. Oxygen consumption data were analyzed by comparing the slope of each time-dependent oxygen profile that excluded the initial 30-min lag necessary for vial equilibration. For all oxygen consumption experiments, a blank sample without embryos and a negative control (embryos exposed to embryo media alone) were included. All samples were analyzed using a linear regression and the blank slope was subtracted from the slope of each treatment.

ATP pre-treatment assay

Embryos (10 embryos per well) were exposed to 100 μl of vehicle (embryo media, as ATP is soluble in water) or ATP (5 or 10 mM) from 0.75 to 2 hpf within clear 96-well plates (Corning Incorporated, Corning, New York). At 2 hpf, embryos were removed from wells and transferred to petri dishes (10 embryos per petri dish; three replicate petri dishes per treatment) containing vehicle (0.1% DMSO) or 0.313 μM niclosamide. At 6 hpf, embryos were removed from treatment solution and assessed for epiboly progression as described above.

mRNA-sequencing

Embryos (10 embryos per petri dish; nine petri dishes per treatment) were exposed under static conditions at 28°C to 10 ml of vehicle (0.1% DMSO) or 0.313 μM niclosamide from (1) 2 to 6 hpf or 4 to 6 hpf and (2) 2 to 3, 2 to 4, 2 to 5, or 2 to 6 hpf. Surviving embryos (30 per replicate pool; triplicate pools per treatment) were snap-frozen in liquid nitrogen at the end of each exposure, and then stored at −80°C until RNA extraction. Triplicate pools of 30 embryos per pool were homogenized in 2-ml cryovials using a PowerGen Homogenizer (Thermo Fisher Scientific, Waltham, Massachusetts), resulting in a total of 36 samples. Following homogenization, a SV Total RNA Isolation System (Promega, Madison, Wisconsin) was used to extract total RNA from each replicate sample per manufacturer's instructions.

Libraries were prepared using a QuantSeq 3′ mRNA-Seq Library Prep Kit FWD (Lexogen, Vienna, Austria) and indexed by treatment replicate per manufacturer's instructions. Library quality and quantity were confirmed using our Qubit 3.0 Fluorometer and 2100 Bioanalyzer system, respectively. Libraries from two exposure scenarios were then pooled (12 libraries per pool), diluted to a concentration of 1.3 pM (with 1% PhiX control), and single-read (1 × 75) sequenced on our Illumina MiniSeq Sequencing System (San Diego, California) using three separate 75-cycle High-Output Reagent Kits. All sequencing data were uploaded to Illumina's BaseSpace in real-time for downstream analysis of quality control. Raw Illumina (fastq.gz) sequencing files (36 files totaling 8.24 GB) are available via NCBI's BioProject database under BioProject ID PRJNA454154, and a summary of sequencing run metrics are provided in Supplementary Table 1 (≥92.41% of reads were ≥Q30). All 36 raw and indexed Illumina (fastq.gz) sequencing files were downloaded from BaseSpace, and uploaded to Bluebee's genomics analysis platform. Quality trimming of reads was performed within Bluebee using BBDuk (v35.92). Trimmed reads were aligned against the current zebrafish genome assembly (GRCz10) using STAR Aligner (v2.5.2a) with modified ENCODE settings. Aligned reads were then indexed, counted, and mapped using Samtools (v1.3), HTSeq-count (v0.6.0), and RSeQC (v2.6.4), respectively.

For 2- to 6-hpf and 4- to 6-hpf exposures, a DESeq2 application within Bluebee (Lexogen Quantseq DE 1.2) was used to identify significant treatment-related effects on transcript abundance (relative to vehicle controls) based on a false discovery rate (FDR) p-adjusted value $<.05$. Using DESeq2-identified transcripts, downstream analyses were run using Qiagen's Ingenuity Pathway Analysis (IPA). Statistically significant transcripts were uploaded to IPA, and human, rat, and mouse homologs were automatically identified within IPA using NCBI's HomoloGene. An Expression Analysis was then performed using a Fisher's Exact Test p-value threshold of .05 as the basis for identifying statistically significant pathways; the algorithm considered both direct and indirect relationships using Ingenuity Knowledge Base (genes only) as the reference set.

To identify potential effects on maternal transcript degradation and zygotic genome activation, vehicle (0.1% DMSO) and niclosamide (0.313 μM) libraries from 2- to 3-, 2- to 4-, 2- to 5-, and 2- to 6-hpf exposures were normalized in Bluebee's DESeq2 application (Lexogen Quantseq DE 1.2). A list of zebrafish-specific maternal and zygotic transcripts were obtained from the literature (Harvey *et al.*, 2013), and the sum of DESeq2-normalized read counts was calculated for zygotic and maternal transcripts within each library.

Whole-mount immunohistochemistry

Embryos (10 embryos per petri dish; nine replicate petri dishes per treatment) were exposed under static conditions 28°C from 2 to 6 hpf or 4 to 6 hpf to 3 ml of vehicle (0.1% DMSO) or niclosamide (0.313 μM). At 6 hpf, embryos were removed from treatment solution, dechorionated by incubating in 10 mg/ml pronase for 10 min, pooled (30 per pool; three replicate pools), and fixed overnight in 4% paraformaldehyde/1× phosphate-buffered saline (PBS). Fixed embryos were labeled using a 1:100 dilution of zebrafish-reactive anti-acetylated α-tubulin (Sigma) antibody and 1:500 dilution of Alexa Fluor 555-conjugated goat anti-mouse IgG2b (ThermoFisher Scientific). Stained embryos were imaged using a Leica MZ10 F stereomicroscope equipped with a DMC2900 camera. Tubulin fluorescence in the yolk sac, cell mass, and whole embryo was quantified using the Corrected Total Cell Fluorescence method for ImageJ (v1.51m9) (McCloy *et al.*, 2014).

In vitro tubulin polymerization assay

A fluorescence-based porcine brain tubulin polymerization assay (Cytoskeleton, Inc.) was used to determine whether niclosamide interferes with polymerization of tubulin into microtubules *in vitro*. The rate of polymerization in the presence of vehicle (0.1% DMSO), 3 μM nocodazole (a known inhibitor of tubulin polymerization), or niclosamide (1.56–200 μM) was quantified in kinetic mode using a GloMax Multiplus Plate Reader (Promega) per manufacturer's instructions.

Statistical analysis

For all data, a general linear model (GLM) analysis of variance (ANOVA) ($\alpha = .05$) was performed using SPSS Statistics 24, as these data did not meet the equal variance assumption for non-GLM ANOVAs. Treatment groups were compared with vehicle controls, and time-points for recovery and sensitivity window assays were compared with 2- to 6-hpf exposures using

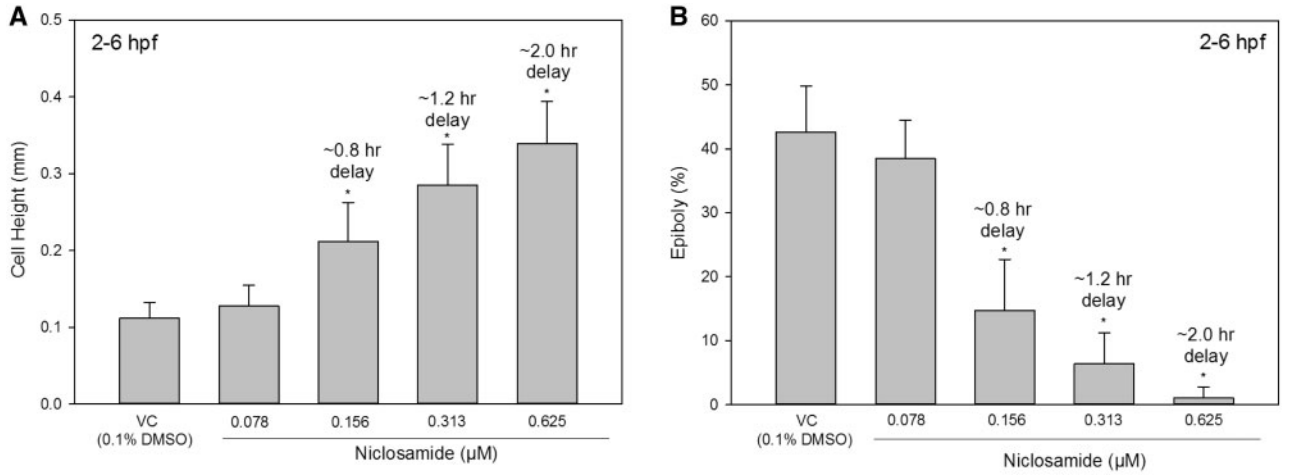

Figure 1. Initiation of exposure to niclosamide at 2 hpf results in epiboly delay at 6 hpf. Epiboly progression was quantified as cell height (mm) above yolk sac (A) and cell progression over yolk sac/total yolk height*100 (or percent epiboly). (B) Data represent three-independent replicate treatments (10 embryos per replicate) and are presented as mean ± standard deviation. Asterisk denotes significant ($p < .05$) difference relative to vehicle control.

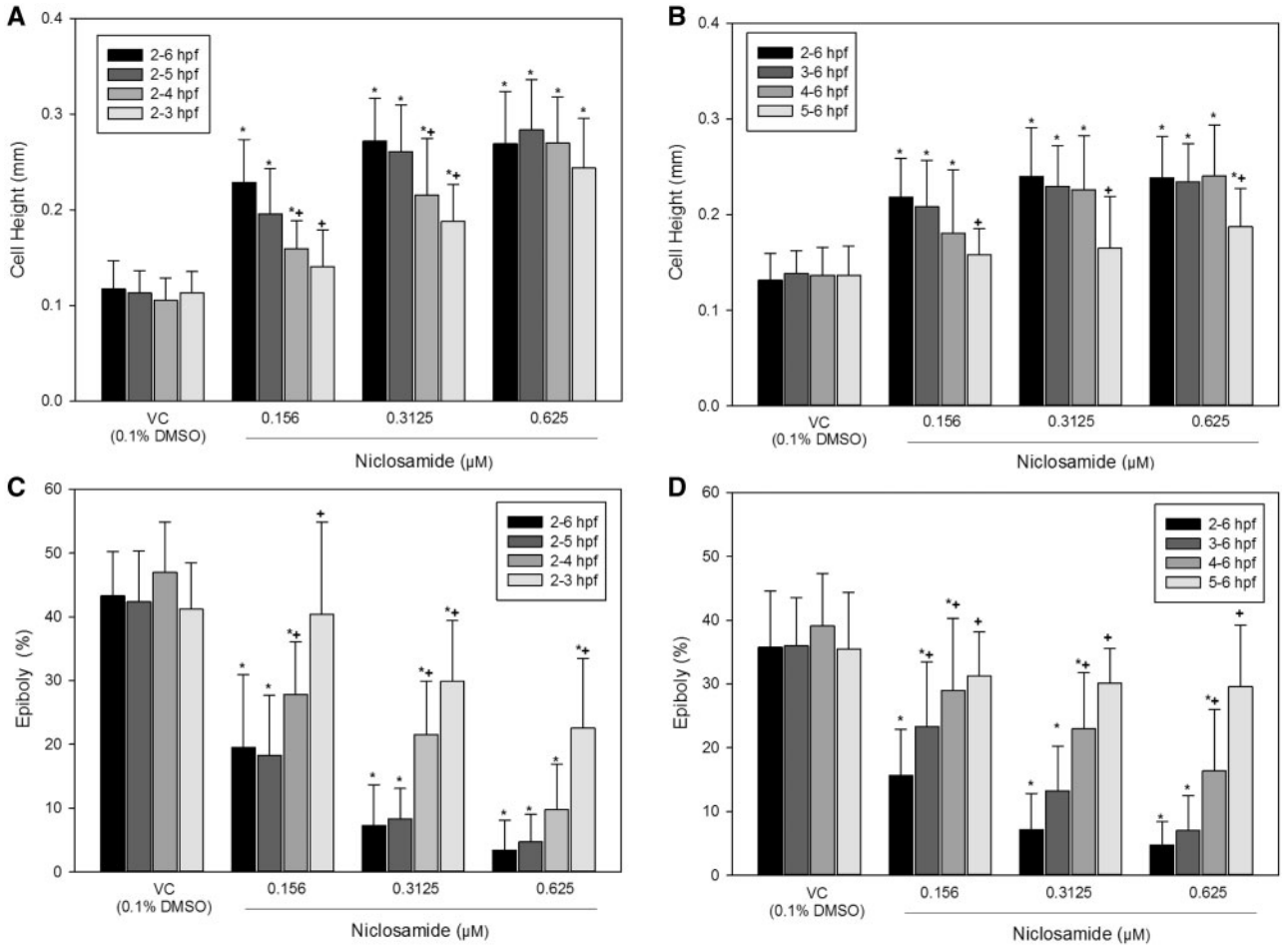

Figure 2. Niclosamide induces a delay in epiboly progression—an effect that increases in severity with longer exposure duration (A and B) and earlier exposure initiation. (C and D) Epiboly progression was quantified as cell height (mm) above yolk sac and percent epiboly (cell progression over yolk sac/total yolk length). Data represent three-independent replicate treatments (10 embryos per replicate) and are presented as mean ± standard deviation.

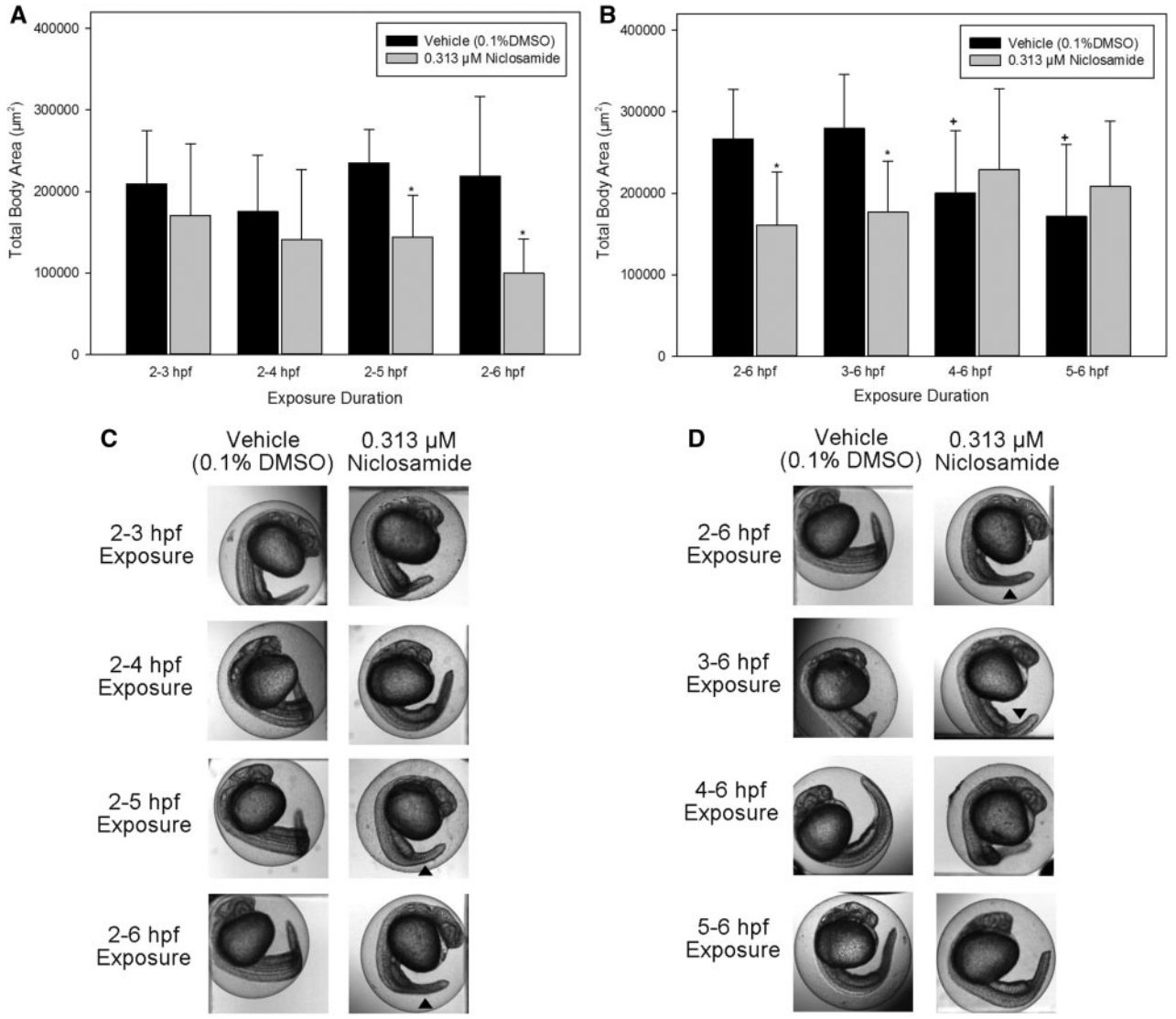

Figure 3. Exposure to 0.313 µM niclosamide from 2 to 5 hpf, 2 to 6 hpf, or 3 to 6 hpf results in a significant decrease in total body area at 24 hpf. Panels A and B summarize data from recovery and sensitive window experiments, respectively, and are based on a sample size of 16 embryos per exposure scenario. Independent 2- to 6-hpf exposures were conducted for recovery and sensitive window experiments to reflect maximum exposure durations; relative to embryos exposed to vehicle from 2 to 6 hpf, total body area was significantly decreased in both experiments following exposure to 0.313 µM niclosamide from 2 to 6 hpf. Data are presented as mean ± standard deviation. Asterisk denotes significant ($p < .05$) difference in niclosamide-treated embryos relative to vehicle controls within the same exposure scenario. Cross (+) denotes significant ($p < .05$) within-treatment difference relative to the 2- to 6-hpf exposure scenario. Representative transmitted light images of 24-hpf embryos for each exposure scenario are shown in Panels C and D. Stunted tails (black arrows) are visible within embryos exposed to 0.313 µM niclosamide from 2 to 5 hpf, 2 to 6 hpf, or 3 to 6 hpf.

pair-wise Tukey-based multiple comparisons of least square means to identify significant differences.

RESULTS

Niclosamide Induces a Concentration-Dependent Delay in Epiboly Progression

We first exposed embryos to a range of niclosamide concentrations (0.078–10 µM) from 2 to 6 hpf, and determined that exposure to niclosamide resulted in a concentration-dependent arrest in epiboly at 6 hpf and increase in mortality at 24 hpf; at concentrations 2.5 µM or higher, 100% mortality was observed at 24 hpf (data not shown). Exposure to lower niclosamide concentrations resulted in a concentration-dependent delay in epiboly progression, with a significant (~0.8 h) delay starting at 0.156 µM (Figs. 1A and 1B). Moreover, we found that niclosamide-induced effects on epiboly at 6 hpf were dependent on niclosamide concentration and exposure duration. When exposed to 0.156 and 0.313 µM niclosamide, partial to full recovery occurred in the 2- to 4-hpf and 2- to 3-hpf exposure groups, respectively, relative to 2- to 6-hpf exposures (Figs. 2A and 2C). In addition, after initiating exposure every hour to identify sensitive windows of niclosamide exposure, we found that initiation of niclosamide exposure at 2 or 3 hpf resulted in a higher magnitude of epiboly delay at 6 hpf (Figs. 2B and 2D).

When embryos were exposed to niclosamide from 2 to 5 hpf, 2 to 6 hpf, or 3 to 6 hpf followed by incubation in clean media until 24 hpf, we found that total body area was significantly decreased within 24-hpf embryos, whereas total body area was not significantly decreased in embryos exposed from 4 to 6 hpf or 5 to 6 hpf (Figure 3). Collectively, these phenotypic

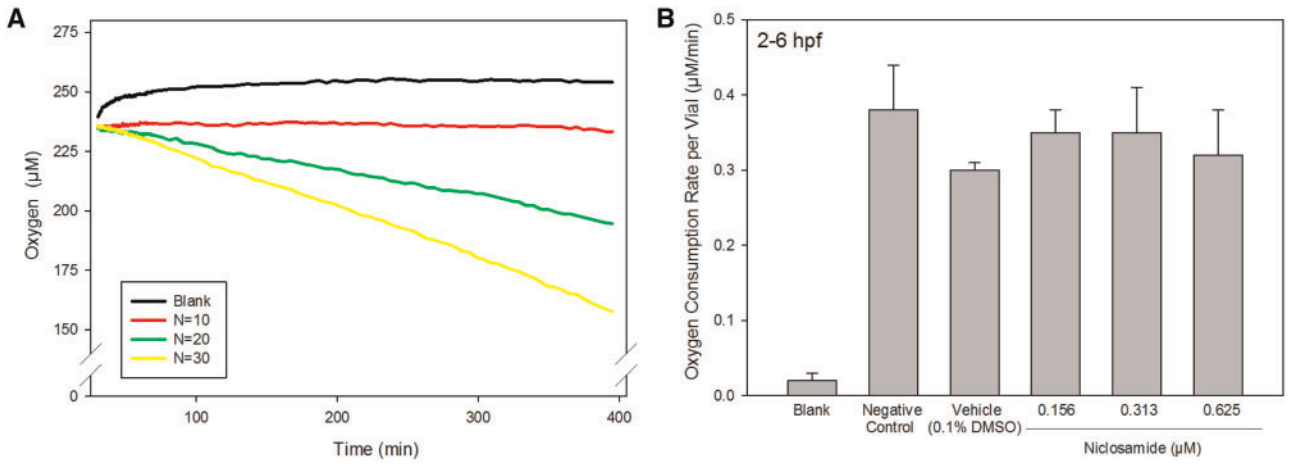

Figure 4. Exposure to niclosamide from 2 to 6 hpf does not significantly alter oxygen consumption rates over a 400-min period following exposure. In Panel A, data are presented as oxygen consumption profiles of vials containing either embryo media alone (blank), or groups of 10, 20, or 30 embryos per vial. In Panel B, data are presented as mean oxygen consumption rate ± standard deviation across four-independent replicates containing either embryo media alone (blanks) or 20 embryos per vial.

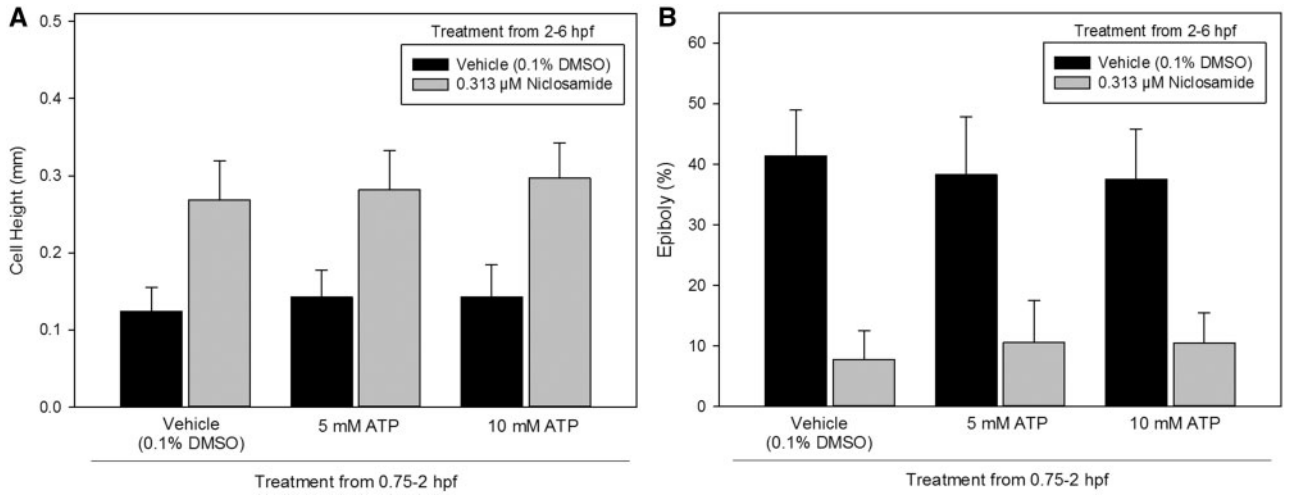

Figure 5. Pre-treatment with 5 or 10 mM ATP from 0.75 to 2 hpf does not significantly mitigate epiboly delay following exposure to 0.313 μM niclosamide from 2 to 6 hpf. Epiboly progression represented as (A) cell height above yolk sac and (B) percent epiboly (cell progression over yolk sac/total yolk length*100). Data represent the mean ± standard deviation of three-independent replicates, with a sample size of 10 embryos per replicate.

assessments demonstrate that niclosamide exposure results in epiboly delay in a concentration- and exposure duration-dependent manner, and that the susceptible window of niclosamide exposure is within blastula.

Niclosamide Does Not Significantly Alter Embryo Oxygen Consumption

To test the hypothesis that niclosamide-induced epiboly delay may be due to effects on OXPHOS, we assessed the ability of niclosamide to interfere with oxygen consumption at early stages of embryonic development using vials containing oxygen-sensitive sensors. A density of 20 embryos per vial was identified as optimal based on preliminary experiments comparing oxygen consumption rates using 10, 20, and 30 embryos per vial (Figure 4A and Supplementary Table 2). Embryos exposed to 0.313 μM from 2 to 6 hpf did not significantly alter oxygen consumption rates over a 400-min period following exposure (Figure 4B and Supplementary Table 3). Overall, these data suggest that niclosamide-induced epiboly delay may not be associated with uncoupling of OXPHOS.

ATP Pre-Treatment Does Not Block Niclosamide-Induced Epiboly Delay

We then tested the hypothesis that niclosamide-induced epiboly delay may be due to decreased ATP production. We first exposed embryos to a range of ATP concentrations (5–50 mM) from 0.75 to 2 hpf, and determined that the maximum tolerated ATP concentration was <25 mM based on the absence of gross malformations and embryo mortality at 6 hpf (data not shown). Therefore, embryos were pre-treated to 5 or 10 mM ATP from 0.75 to 2 hpf and then treated with vehicle (0.1% DMSO) or 0.313 μM niclosamide from 2 to 6 hpf. We found that pre-treatment with ATP did not block nor mitigate niclosamide-induced epiboly delay (Figs. 5A and 5B), suggesting that niclosamide-induced epiboly delay may not be associated with a decrease in embryonic ATP concentrations following niclosamide exposure.

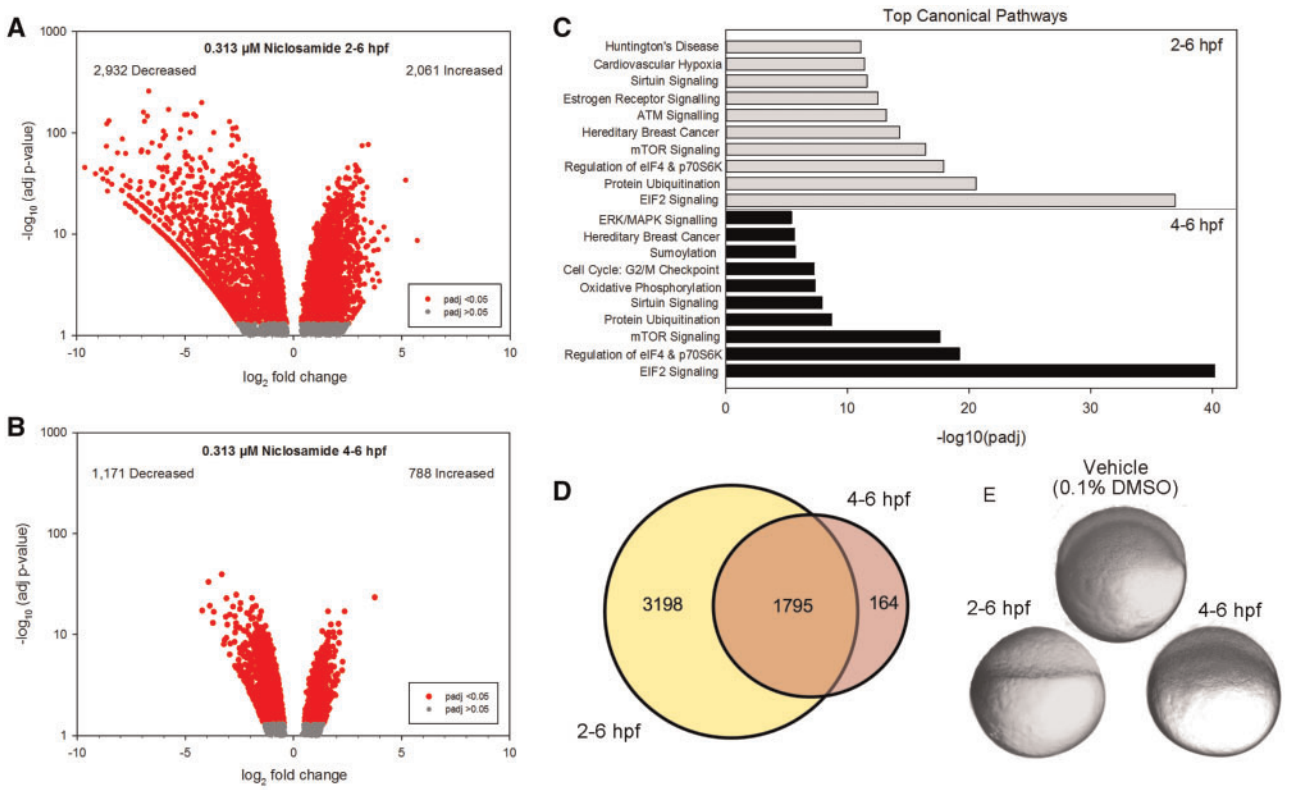

Figure 6. Exposure to 0.313 µM niclosamide from 2 to 6 hpf and 4 to 6 hpf results in significant effects on transcript abundance (A and B) and pathways related to protein synthesis, cell cycle regulation, and various signaling pathways. (C) Volcano plots showing the number of significantly different transcripts within embryos exposed to 0.313 µM niclosamide from 2 to 6 and 4 to 6 hpf, (A and B) with the $\log_2$-transformed fold change on the x-axis and the $-\log_{10}$-transformed *p*-adjusted value on the y-axis. 1795 significantly altered transcripts were common to both exposure durations. (D) Canonical Pathways (C) affected by niclosamide exposure were identified by IPA's Expression-Analysis using a Fisher's exact *p*-value <.05. Panel E shows representative images of embryos exposed to 0.313 µM niclosamide from 2 to 6 and 4 to 6 hpf.

Niclosamide Results in Significant Impacts on the Transcriptome at 6 hpf

Exposure of embryos to 0.313 µM niclosamide from 2 to 6 hpf significantly affected the abundance of 4993 transcripts (relative to vehicle controls) at 6 hpf, where the abundance of 2932 and 2061 transcripts were significantly decreased and increased, respectively (Figure 6A and Supplementary Table 4). Following a 2-h exposure from 4 to 6 hpf, 1959 transcripts were significantly affected (relative to vehicle controls) at 6 hpf, where 1171 and 788 transcripts were significantly decreased and increased, respectively (Figure 6B and Supplementary Table 5). Interestingly, nearly 92% of significantly altered transcripts (1795 total) in the 4- to 6-hpf exposure were also significantly affected in the 2- to 6-hpf exposure (Figure 6D).

Following automated identification of human, rat, or mouse homologs within IPA, approximately 64% (3209 out of 4993) and 66% (1287 out of 1959) of statistically significant transcripts from the 2- to 6-hpf and 2- to 4-hpf exposures, respectively, were included in IPA's analysis; the remaining statistically significant transcripts were excluded by IPA's analysis due to the absence of human, rat, and/or mouse orthologs within NCBI's Homologene database. Interestingly, based on IPA's canonical pathways, both exposure scenarios resulted in significant effects on pathways involved in protein synthesis (Figure 6C and Supplementary Tables 6 and 7). At the transcript-level, the most significantly decreased transcripts were related to the cytoskeleton as well as gastrulation/epiboly and embryonic patterning (Table 1), whereas the most significantly increased transcripts were related to GTP/GDP binding, signal transduction, and cell cycle regulation (Table 1).

Niclosamide Delays Maternal Transcript Degradation and Zygotic Genome Activation

Although exposure to 0.313 µM niclosamide from 2 to 3 or 2 to 4 hpf did not significantly alter the abundance of maternal nor zygotic transcripts at 3 and 4 hpf, respectively, exposure to 0.313 µM niclosamide from 2 to 5 hpf resulted in significantly higher levels of maternal transcripts and significantly lower levels of zygotic transcripts at 5 hpf relative to time-matched vehicle controls (Figure 7 and Supplementary Tables 8 and 9). However, exposure from 2 to 6 hpf did not result in significant differences in maternal and zygotic transcripts at 6 hpf despite a ~1.2-h delay in epiboly at the same time-point. Overall, these data suggest that initiation of niclosamide exposure at 2 hpf delays maternal transcript degradation and zygotic genome activation between 4 and 5 hpf, an effect that may decrease in severity as embryos progress through early-gastrula.

Niclosamide Decreases Tubulin Polymerization In Vitro

Zebrafish embryos exposed to 0.313 µM niclosamide from 2 to 6 hpf or 4 to 6 hpf did not result in a significant effect on tubulin (based on total fluorescence) within the embryo yolk sac, cell mass, or whole embryo (Figure 8A and Supplementary Table 10). These results suggest that niclosamide does not alter the abundance nor localization of tubulin within the zebrafish embryo. However, within an *in vitro* tubulin polymerization assay,

Table 1. Top 25 Significantly Decreased Or Increased Transcripts Ranked by Fold Change for Each Exposure Duration

Category	Gene	Shared	log2 Fold Change	(−)log10 (FDR)	GO Terms
2–6 hpf Top 25 decreased transcripts					
Cytoskeleton	krt92	Y	−9.63	45.32	Cytoskeletal filament
	krt4	N	−8.86	43.21	Cytoskeletal filament
	krt18	N	−8.11	63.26	Cytoskeletal filament
	cyt1l	N	−7.59	18.85	Cytoskeletal filament
	add3b	N	−7.56	28.89	Cytoskeleton
	evpla	Y	−7.53	28.79	Intermediate filament binding
	krt97	N	−7.34	17.09	Cytoskeletal filament
	krt96	Y	−7.23	21.14	Cytoskeletal filament
Epiboly and gastrulation	cldne	N	−8.41	44.12	Epiboly involved in gastrulation
	cyt1	Y	−7.72	30.44	Cell migration involved in gastrulation
Lipid ane membrane	afp4	N	−7.89	26.73	Lipid catabolism
	mtp	N	−7.20	20.86	Lipid metabolism
Development	asb11	N	−8.57	33.32	Notch signaling, protien ubiquination
	tbx16	N	−8.51	131.29	Left/right symmerty
	szl	N	−7.29	16.56	dorsal/ventral signaling
Transcriotion	vgll4l	N	−8.58	26.49	Transcription
	polr3gla	N	−7.90	26.78	Transcription
	sb:cb81	N	−7.53	33.56	UTR-mediated mRNA destabilization
Other	aldob	N	−8.63	73.66	Glycolysis
	fb06f03	N	−8.62	40.44	Fin regeneration
	stm	N	−8.61	122.52	Otic placode formation
	lye	N	−8.38	31.03	Cellular adhesion and signaling
	sox11a	N	−7.51	18.32	Brain development
	zic2b	N	−7.94	27.11	Regulation of retinoic acid receptor signaling
	dnase1l4.1	N	−7.58	24.00	DNA catabolism
2–6 hpf Top 25 increased transcripts					
GTP/GDP	zgc:162879	N	3.13	11.28	GTP binding
	arl4aa	Y	3.08	34.78	GTPase-mediated signal transduction
Cell cycle	moto	N	3.70	6.83	Meiotic cell cycle
	mtus1a	N	2.9	42.0	Cell cycle
	cdc45	N	2.9	36.7	Cell Cycle
	hbegfa	N	3.39	28.95	Cell proliferation
Metabolism	pgp	N	4.32	8.78	Metabolic process
	lipg	N	3.05	33.86	Metabolic process
	zgc:73340	N	3.02	19.81	Metabolic process
Phosphorylation	ulk1a	Y	3.59	13.00	Phosphorylation
	mos	N	3.21	25.35	Phosphorylation
	ctdsp1	N	2.95	11.27	Phosphatase
	arhgap32a	N	2.9	45.4	Phosphorylation
DNA repair	apex2	N	3.28	13.87	DNA repair
	ercc4	N	3.0	19.6	DNA repair
Other	dcun1d4	Y	5.18	34.02	Ubiquitin-protein transferase
	alg13	N	3.61	8.51	Dorsal/ventral pattern formation
	ccdc115	Y	3.42	7.64	Unfolded protien binding
	sytl4	N	3.35	7.41	Intracellular protein transport
	dlg5a	N	3.22	22.17	Apoptosis
	trim35-29	N	3.18	33.56	Carbonate dehydrogenase
	bmb	N	3.17	74.62	Pronuclear fusion
	osbpl3a	N	3.12	5.78	Lipid transport
	asf1bb	N	3.06	32.67	Transcription
	zgc:152977	Y	2.9	12.0	Cytoskeleton
4–6 hpf Top 25 decreased transcripts					
Cytoskeleton	krt17	N	−4.22	17.31	Cytoskeletal filament
	zgc:110712	N	−3.69	16.78	Cytoskeletal filament
	krt5	N	−3.10	22.85	Cytoskeletal filament
	krt96	Y	−2.95	15.78	Cytoskeletal filament
	zgc:110333	N	−2.93	8.15	Structural activity
	evpla	Y	−2.79	18.91	Intermediate filament binding
	krt92	Y	−2.65	24.74	Cytoskeletal filament
	tmsb1	N	−2.63	12.13	Actin filament organization

Continued

Table 1. (continued)

Category	Gene	Shared	log2 Fold Change	(−)log10 (FDR)	GO Terms
Epiboly and gastrulation	cyt1	Y	−3.93	33.12	Cell migration involved in gastrulation
	apoc1	N	−3.32	39.45	Cell migration involved in gastrulation
Lipid and membrane	zgc:101640	N	−2.69	10.47	Phospholipid transport
	mal2	N	−3.23	8.04	Membrane integrity
	zgc:91849	N	−2.50	7.32	Membrane integrity
Development	her7	N	−3.73	13.03	Anterior/posterior patterning
	efnb2a	N	−2.72	8.45	Anterior/posterior patterning
	mespab	N	−2.66	4.70	Somite rostral/caudal axis specification
Other	cd44a	N	−2.49	4.96	Cell adhesion
	hk1	N	−2.52	4.39	Glycolysis
	rabgap1l2	N	−2.65	11.77	Intracellular protein transport
	anxa1c	N	−2.68	4.77	Calcium ion binding
	fut9d	N	−2.69	4.83	Protein glycosylation
	sox2	N	−2.70	4.88	Fin regeneration
	hsd17b14	N	−2.71	15.13	Oxioreductase activity
	znf750	N	−2.95	6.35	Cell differentiation
	im:7150988	N	−3.19	8.81	Cellular response to xenobiotics
4–6 hpf Top 25 increased transcripts					
GTP/GDP	arl4aa	Y	1.95	2.50	GTPase-mediated signal transduction
Cell cycle	btg4	N	2.10	8.25	Cell proliferation
	cdca9	N	1.73	2.73	Cell division
	zw10	N	1.70	4.58	Mitotic cell cycle
Lipid and membrane	zgc:113425	N	2.14	10.47	Membrane component
	si:ch211157b11.12	N	1.86	6.05	Membrane component
	vps9d1	N	1.84	3.38	Membrane component
Cytoskeleton	zgc:152977	Y	1.74	12.55	Cytoskeletal anchoring
	zgc:56231	N	1.94	3.92	Microtubule-based movement
Protien transport	snx10a	N	1.90	9.43	Protien transport
	stx11a	N	1.77	2.42	Protein transport
Other	egln3	N	3.77	23.38	REDOX processes
	si:rp71-45k5.2	N	2.37	16.97	Transcription
	ccdc15	Y	2.28	5.36	Unfolded protien binding
	igfbp1a	N	2.26	4.42	Response to hypoxia
	dcun1d4	Y	2.09	12.76	Ubiquitin-protein transferase
	cbx8b	N	2.05	4.05	Hematopoietic progenitor cell differentiation
	ulk1a	Y	2.04	3.50	Phosphorylation
	gfod2	N	1.88	4.80	Oxioreductase activity
	mier3b	N	1.87	6.12	DNA binding
	micall2b	N	1.84	10.51	Endocytic recycling
	cyp1b1	N	1.83	7.63	Xenobiotic metabolic process
	pim2	N	1.74	4.93	Apoptosis
	josd2	N	1.71	2.66	CNS morphogenesis
	tbpl2	N	1.71	2.46	Embryo pattern specification

Gene Ontology (GO) terms were retrieved from The Zebrafish Information Network (http://zfin.org).

niclosamide resulted in a concentration-dependent decrease in tubulin polymerization starting at 12.5 μM niclosamide (Figure 8B), suggesting that niclosamide may be inhibiting the formation of microtubule networks *in vitro*.

DISCUSSION

Epiboly is characterized by spreading of the cell mass over the yolk sac—an important process that plays a prominent role in embryo gastrulation and specification of the dorsoventral axis (Kimmel *et al.*, 1995; Lepage and Bruce, 2010). Epiboly is a process that is shared among vertebrates (Solnica-Krezel, 2005), and epiboly delay is an adverse outcome that has been observed in response to a wide range of compounds, many of which are thought to target the mitochondrial electron transport chain (Lai *et al.*, 2013; Legradi *et al.*, 2017; Mendelsohn and Gitlin, 2008). In this study, we demonstrated that exposure to niclosamide during early zebrafish embryogenesis resulted in a concentration-dependent delay in epiboly progression ranging from ~0.8 to 2.0 h relative to vehicle controls, an effect that was more severe with increasing exposure duration and increasingly early exposure initiation.

Given that mitochondrial OXPHOS is responsible for the majority of oxygen metabolism and ATP production within complex organisms and oxygen consumption directly reflects OXPHOS (Stackley *et al.*, 2011), we first leveraged oxygen consumption as a simple, non-invasive readout to evaluate potential OXPHOS dysfunction (Legradi *et al.*, 2017; Raheem *et al.*, 1980; Tao *et al.*, 2014; Wilson *et al.*, 1983). Whereas niclosamide-induced epiboly delay may be indicative of OXPHOS uncoupling, embryos exposed to 0.313 μM

niclosamide from 2 to 6 hpf did not significantly alter oxygen consumption rates over a 400-min period within clean media from 6 to 13 hpf. In addition, ATP pre-treatment prior to niclosamide exposure did not mitigate niclosamide-induced epiboly delay. As increased oxygen consumption and inhibition of ATP production are downstream consequences of OXPHOS uncoupling, our data suggest that niclosamide-induced epiboly delay may not be a result of OXPHOS disruption but, rather, may be acting through an alternative mechanism (Bestman *et al.*, 2015).

The maternal-to-zygotic transition (MZT) within an embryo represents the transition from reliance on maternally derived transcripts to *de novo* transcription of the zygotic genome. The MZT occurs in all animals and involves a host of changes in the developing embryo, including initiation of cell motility (Kimmel *et al.*, 1990; Langley *et al.*, 2014; Yartseva and Giraldez, 2015). In zebrafish, this transition occurs from ~2 to 3 hpf and is required for epiboly progression (Kane *et al.*, 1996; Kimmel *et al.*, 1995; Langley *et al.*, 2014). In our study, exposure to niclosamide from 2 to 5 hpf or 2 to 6 hpf resulted in a more severe effect on epiboly progression relative to niclosamide exposure from 2 to 3 hpf or 2 to 4 hpf. In addition, initiation of niclosamide exposure at 2 or 3 hpf resulted in a more severe effect on epiboly progression and embryonic development by 24 hpf relative to exposures initiated at 4 or 5 hpf. Collectively, these data suggest the sensitive window of niclosamide exposure is within blastula, a period of development that encompasses the MZT. Indeed, niclosamide exposure resulted in significant increases in transcripts specific to transcriptional processes, suggesting that niclosamide may be targeting processes involved in the initiation of the MZT.

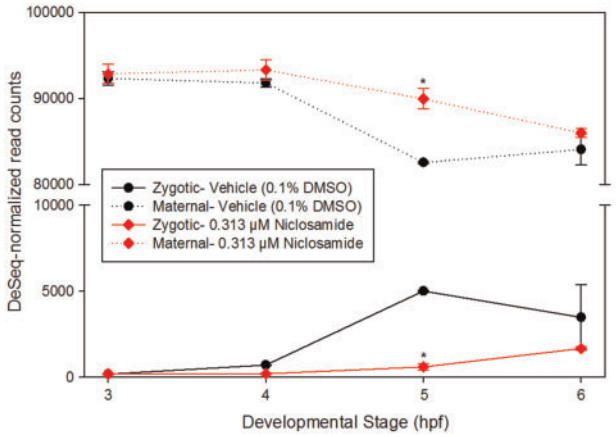

Figure 7. Exposure to 0.313 µM niclosamide from 2 to 5 hpf results in a significant delay in maternal transcript degradation and zygotic genome activation. Data represent the mean ± standard deviation of total DESeq-normalized read counts across three replicate libraries per treatment. Asterisk denotes significant ($p < .05$) difference relative to time-matched vehicle controls.

We then tested the hypothesis that niclosamide exposure blastula and early-gastrula leads to effects on maternal transcript degradation and zygotic genome activation. Indeed, initiation of exposure to niclosamide at the beginning of the MZT (2 hpf) resulted in an increased abundance of maternal transcripts and decreased abundance of zygotic transcripts at 5 hpf relative to time-matched vehicle controls, suggesting that niclosamide may delay maternal transcript degradation and zygotic genome activation. However, maternal and zygotic transcripts were not significantly different at 6 hpf following a 2- to 6-hpf exposure, suggesting that impacts to both sets of transcripts may decrease in severity as embryos progress through early-gastrula. As zygotic transcription is essential for epiboly initiation and progression (Kane *et al.*, 1996; Lepage and Bruce, 2010), niclosamide-induced delays in zygotic genome activation may be responsible for downstream delays in epiboly—effects that may be a direct consequence of delays in maternal transcript degradation. Among the most abundant maternal transcription factors present within developing embryos are *nanog*, *sox19b*, and *pou5f1*, all of which have been shown to regulate zygotic genome activation in zebrafish (Lee *et al.*, 2013). Indeed, niclosamide exposure resulted in significant impacts on *nanog*, *sox19b*, and *pou5f1* transcripts following a 2- to 6-hpf exposure, suggesting that niclosamide may disrupt transcript levels of key maternal transcription factors involved in zygotic genome activation and epiboly progression.

In addition to delays in maternal transcript degradation and zygotic genome activation, our mRNA-sequencing data demonstrated that numerous cytoskeleton-related transcripts were significantly altered following niclosamide exposure from 2 to 6

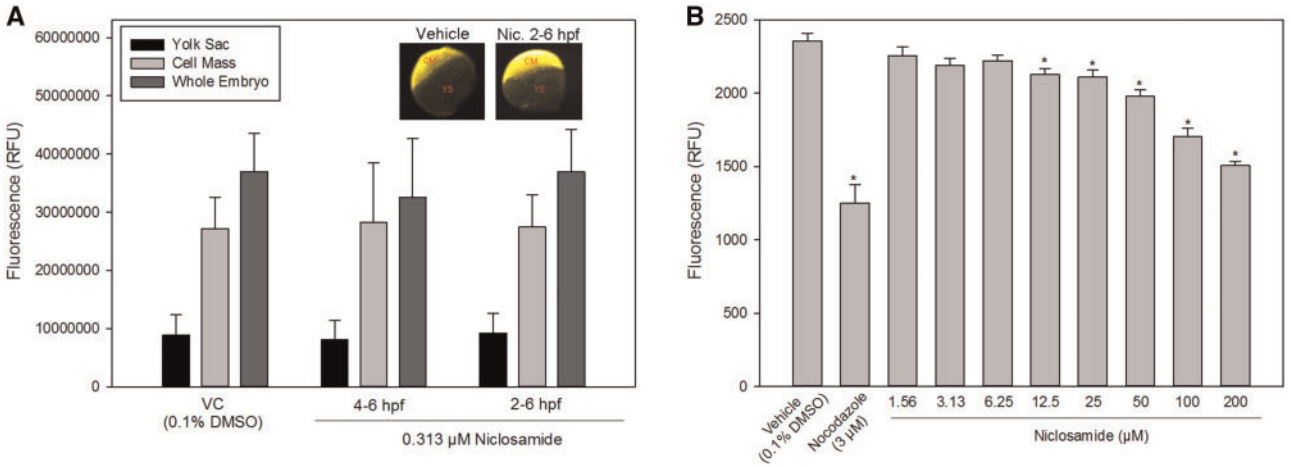

Figure 8. Niclosamide exposure from 2 to 6 hpf or 4 to 6 hpf does not significantly affect tubulin abundance nor localization in the yolk sac, cell mass, or whole embryo, (A) whereas niclosamide results in a significant, concentration-dependent decrease in tubulin polymerization *in vitro*. (B) Fluorescence data within Panel A are presented as mean fluorescence (relative fluorescence units, or RFU) ± standard deviation across 20 embryos. *In vitro* tubulin polymerization data within Panel B are presented as mean fluorescence (RFU) ± standard deviation across four-independent replicates. Nocodazole was used as a positive control for inhibition of tubulin polymerization. CM, cell mass; YS, yolk sac.

hpf, including beta (*tubb2b*) and alpha (*tuba1a*, *tuba1b*, *tuba8l4*, and *tuba4l*) tubulin transcripts, suggesting that the cytoskeleton may be affected within epiboly-delayed embryos exposed to niclosamide. Prior studies have demonstrated that movement of the blastoderm around the yolk sac occurs through interactions with microtubules present in the yolk sac (Solnica-Krezel and Driever, 1994; Strahle and Jesuthasan, 1993), and epiboly progression in zebrafish embryos is dependent on the presence of intact yolk sac microtubules that shorten as epiboly progresses (Jesuthasan and Stähle, 1997). Our whole-mount immunohistochemistry data suggest that niclosamide does not impact the abundance nor localization of tubulin from the yolk sac or embryonic blastodisc (cell mass). However, our *in vitro* tubulin polymerization data suggest that niclosamide inhibits polymerization of tubulin dimers into microtubules.

In conclusion, this study demonstrated that (1) niclosamide exposure during early zebrafish embryogenesis results in a concentration-dependent delay in epiboly that may be independent of OXPHOS disruption; (2) the window of sensitivity for niclosamide exposure is within blastula and coincides with the timing of the MZT; (3) niclosamide delays degradation of maternal transcripts and initiation of zygotic genome activation; and (4) niclosamide results in a concentration-dependent decrease in tubulin polymerization *in vitro*. Overall, our data suggest that niclosamide may be preventing the progression of epiboly by disrupting the timing of zygotic genome activation, an effect that may be mediated through disruption of maternal transcription factors and/or microtubule polymerization. Therefore, future studies are needed to (1) confirm the potential target and mechanism of action for niclosamide within zebrafish embryos and (2) determine whether similar effects on epiboly occur *in utero* within mammalian models following non-oral routes of niclosamide exposure.

SUPPLEMENTARY DATA

Supplementary data are available at *Toxicological Sciences* online.

FUNDING

This work was supported by UCR's Graduate Division and NRSA T32 Training Program (T32ES018827) to S.M.V, as well as a National Institutes of Health grant (R01ES027576) and the USDA National Institute of Food and Agriculture Hatch Project (1009609) to D.C.V.

ACKNOWLEDGMENTS

We gratefully thank Chloe Pham for her assistance with sorting and staging zebrafish embryos. We also gratefully thank Teresa Schwemmer, Adelle Molina, and Janet Nye (Stony Brook University) for their assistance in analyzing oxygen consumption data.

REFERENCES

Andrews, P., Thyssen, J., and Lorke, D. (1982). The biology and toxicology of molluscicides, Bayluscide. *Pharmacol. Ther.* **19**, 245–295.

Balgi, A. D., Fonseca, B. D., Donohue, E., Tsang, T. C. F., Lajoie, P., Proud, C. G., Nabi, I. R., and Roberge, M. (2009). Screen for chemical modulators of autophagy reveals novel therapeutic inhibitors of mTORC1 signaling. *PLoS One* **4**, e7124.

Bestman, J. E., Stackley, K. D., Rahn, J. J., Williamson, T. J., and Chan, S. S. L. (2015). The cellular and molecular progression of mitochondrial dysfunction induced by 2,4-dinitrophenol in developing zebrafish embryos. *Differentiation* **89**, 51–69.

Cairns, D. M., Boorgu, D. S. S. K., Levin, M., and Kaplan, D. L. (2018). Niclosamide rescues microcephaly in a humanized *in vivo* model of Zika infection using human induced neural stem cells. *Biol. Open* **7**, bio031807.

Chen, W., Mook, R. A., Premont, R. T., and Wang, J. (2018). Niclosamide: Beyond an antihelminthic drug. *Cell Signal.* **41**, 89–96.

Chen, M., Wang, J., Lu, J., Bond, M. C., Ren, X.-R., Lyerly, H. K., Barak, L. S., and Chen, W. (2009). The anti-helminthic niclosamide inhibits Wnt/Frizzled1 signaling. *Biochemistry (Moscow)* **48**, 10267–10274.

Duhm, B., Maul, W., Medenwald, H., Patzschke, K., and Wegner, L. A. (1961). Radioaktive Untersuchungen mit einem neuen Molluscicid. *Z. Naturforsch.* **16**, 509–515.

Gwisai, T., Hollingsworth, N. R., Cowles, S., Tharmalingam, N., Mylonakis, E., Fuchs, B. B., and Shukla, A. (2017). Repurposing niclosamide as a versatile antimicrobial surface coating against device-associated, hospital-acquired bacterial infections. *Biomed. Mater. Bristol Engl.* **12**, 045010.

Harvey, S. A., Sealy, I., Kettleborough, R., Fenyes, F., White, R., Stemple, D., Smith, J. C. (2013). Identification of the zebrafish maternal and paternal transcriptomes. *Development* **140**(13), 2703–10.

Imperi, F., Massai, F., Pillai, C. R., Longo, F., Zennaro, E., Rampioni, G., Visca, P., and Leoni, L. (2013). New life for an old drug: The anthelmintic drug niclosamide inhibits *Pseudomonas aeruginosa* quorum Sensing. *Antimicrob. Agents Chemother.* **57**, 996–1005.

Jesuthasan, S., and Stähle, U. (1997). Dynamic microtubules and specification of the zebrafish embryonic axis. *Curr. Biol.* **7**, 31–42.

Jin, Y., Lu, Z., Ding, K., Li, J., Du, X., Chen, C., Sun, X., Wu, Y., Zhou, J., and Pan, J. (2010). Antineoplastic mechanisms of niclosamide in acute myelogenous leukemia stem cells: Inactivation of the NF-B pathway and generation of reactive oxygen species. *Cancer Res.* **70**, 2516–2527.

Kane, D. A., Hammerschmidt, M., Mullins, M. C., Maischein, H. M., Brand, M., van Eeden, F. J., Furutani-Seiki, M., Granato, M., Haffter, P., and Heisenberg, C. P. (1996). The zebrafish epiboly mutants. *Development* **123**, 47–55.

Kimmel, C. B., Ballard, W. W., Kimmel, S. R., Ullmann, B., and Schilling, T. F. (1995). Stages of embryonic development of the zebrafish. *Dev. Dyn.* **203**, 253–310.

Kimmel, C. B., Warga, R. M., and Schilling, T. F. (1990). Origin and organization of the zebrafish fate map. *Development* **108**, 581–594.

Lai, K., Selinger, D. W., Solomon, J. M., Wu, H., Schmitt, E., Serluca, F. C., Curtis, D., and Benson, J. D. (2013). Integrated compound profiling screens identify the mitochondrial electron transport chain as the molecular target of the natural products manassantin, sesquicillin, and arctigenin. *ACS Chem. Biol.* **8**, 257–267.

Langley, A. R., Smith, J. C., Stemple, D. L., and Harvey, S. A. (2014). New insights into the maternal to zygotic transition. *Development* **141**, 3834–3841.

Lee, M. T., Bonneau, A. R., Takacs, C. M., Bazzini, A. A., DiVito, K. R., Fleming, E. S., and Giraldez, A. J. (2013). Nanog, Pou5f1 and

SoxB1 activate zygotic gene expression during the maternal-to-zygotic transition. *Nature* **503**, 360–364.

Lee, S., Son, A.-R., Ahn, J., and Song, J.-Y. (2014). Niclosamide enhances ROS-mediated cell death through c-Jun activation. *Biomed. Pharmacother.* **68**, 619–624.

Legradi, J., Pomeren, M., Dahlberg, A.-K., and Legler, J. (2017). Effects of hydroxylated polybrominated diphenyl ethers in developing zebrafish are indicative of disruption of oxidative phosphorylation. *Int. J. Mol. Sci.* **18**, 970.

Lepage, S. E., and Bruce, A. E. E. (2010). Zebrafish epiboly: Mechanics and mechanisms. *Int. J. Dev. Biol.* **54**, 1213–1228.

Li, Z., Brecher, M., Deng, Y.-Q., Zhang, J., Sakamuru, S., Liu, B., Huang, R., Koetzner, C. A., Allen, C. A., Jones, S. A., *et al.* (2017). Existing drugs as broad-spectrum and potent inhibitors for Zika virus by targeting NS2B-NS3 interaction. *Cell Res.* **27**, 1046–1064.

Li, Y., Li, P.-K., Roberts, M. J., Arend, R. C., Samant, R. S., and Buchsbaum, D. J. (2014). Multi-targeted therapy of cancer by niclosamide: A new application for an old drug. *Cancer Lett.* **349**, 8–14.

Lu, D., Ma, Z., Zhang, T., Zhang, X., and Wu, B. (2016). Metabolism of the anthelmintic drug niclosamide by cytochrome P450 enzymes and UDP-glucuronosyltransferases: Metabolite elucidation and main contributions from CYP1A2 and UGT1A1. *Xenobiotica* **46**, 1–13.

McCloy, R. A., Rogers, S., Caldon, C. E., Lorca, T., Castro, A., and Burgess, A. (2014). Partial inhibition of Cdk1 in G phase overrides the SAC and decouples mitotic events. *Cell Cycle* **13**, 1400–1412.

Mendelsohn, B. A., and Gitlin, J. D. (2008). Coordination of development and metabolism in the pre-midblastula transition zebrafish embryo. *Dev. Dyn.* **237**, 1789–1798.

Pan, J.-X., Ding, K., and Wang, C.-Y. (2012). Niclosamide, an old antihelminthic agent, demonstrates antitumor activity by blocking multiple signaling pathways of cancer stem cells. *Chin. J. Cancer* **31**, 178–184.

Park, J. P., and Fioravanti, C. F. (2006). Catalysis of NADH→NADP+ transhydrogenation by adult *Hymenolepis diminuta* mitochondria. *Parasitol. Res.* **98**, 200.

Raheem, K. A., El-Gindy, H., and Al-Hassan, J. (1980). Interrelationship of molluscicidal concentration and temperature on the respiration of *Bulinus truncatus*. *Hydrobiologia* **74**, 11–15.

Rajamuthiah, R., Fuchs, B. B., Conery, A. L., Kim, W., Jayamani, E., Kwon, B., Ausubel, F. M., and Mylonakis, E. (2015). Repurposing salicylanilide anthelmintic drugs to combat drug resistant *Staphylococcus aureus*. *PLoS One* **10**, e0124595.

Ren, X., Duan, L., He, Q., Zhang, Z., Zhou, Y., Wu, D., Pan, J., Pei, D., and Ding, K. (2010). Identification of niclosamide as a new small-molecule inhibitor of the STAT3 signaling pathway. *ACS Med. Chem. Lett.* **1**, 454–459.

Solnica-Krezel, L. (2005). Conserved patterns of cell movements during vertebrate gastrulation. *Curr. Biol.* **15**, R213–R228.

Solnica-Krezel, L., and Driever, W. (1994). Microtubule arrays of the zebrafish yolk cell: Organization and function during epiboly. *Development* **120**, 2443–2455.

Stackley, K. D., Beeson, C. C., Rahn, J. J., and Chan, S. S. L. (2011). Bioenergetic profiling of zebrafish embryonic development. *PLoS One* **6**, e25652.

Strahle, U., and Jesuthasan, S. (1993). Ultraviolet irradiation impairs epiboly in zebrafish embryos: Evidence for a microtubule-dependent mechanism of epiboly. *Development* **119**, 909–919.

Suliman, M. A., Zhang, Z., Na, H., Ribeiro, A. L. L., Zhang, Y., Niang, B., Hamid, A. S., Zhang, H., Xu, L., and Zuo, Y. (2016). Niclosamide inhibits colon cancer progression through downregulation of the Notch pathway and upregulation of the tumor suppressor miR-200 family. *Int. J. Mol. Med.* **38**, 776–784.

Tao, H., Zhang, Y., Zeng, X., Shulman, G. I., and Jin, S. (2014). Niclosamide ethanolamine-induced mild mitochondrial uncoupling improves diabetic symptoms in mice. *Nat. Med.* **20**, 1263–1269.

Tharmalingam, N., Port, J., Castillo, D., and Mylonakis, E. (2018). Repurposing the anthelmintic drug niclosamide to combat *Helicobacter pylori*. *Sci. Rep.* **8**, 3701.

Vliet, S. M., Ho, T. C., and Volz, D. C. (2017). Behavioral screening of the LOPAC1280 library in zebrafish embryos. *Toxicol. Appl. Pharmacol.* **329**, 241–248.

Weinbach, E., and Garbus, J. (1969). Mechanism of action of reagents that uncouple oxidative phosphorylation. *Nature* **221**, 1016–1018.

Wilson, D. F., Rumsey, W. L., Green, T. J., and Vanderkooi, J. M. (1983). The oxygen dependenceof mitochondrial oxidative phosphorylation measured by a new optical method for measuring oxygen concentration. *J. Biol. Chem.* **263**, 2712–2718.

Xu, M., Lee, E. M., Wen, Z., Cheng, Y., Huang, W.-K., Qian, X., TCW, J., Kouznetsova, J., Ogden, S. C., Hammack, C., *et al.* (2016). Identification of small-molecule inhibitors of Zika virus infection and induced neural cell death via a drug repurposing screen. *Nat. Med.* **22**, 1101–1107.

Yartseva, V., and Giraldez, A. J. (2015). The maternal-to-zygotic transition during vertebrate development: A model for reprogramming. *Curr. Top. Dev. Biol.* **113**, 191–232.

Yorke, R. E., and Turton, J. A. (1974). Effects of fasciolicidal and anti-cestode agents on the respiration of isolated Hymenolepis mitochondria. *Z. Parasitenkd.* **45**, 1–10.